LBL-15281
Preprint

Lawrence Berkeley Laboratory
UNIVERSITY OF CALIFORNIA

Physics, Computer Science & Mathematics Division

Submitted to Nuclear Instruments and Methods

GATED TIME PROJECTION CHAMBER

Peter Némethy, Piermaria J. Oddone,
Nobukazu Toge, and Akira Ishibashi

November 1982

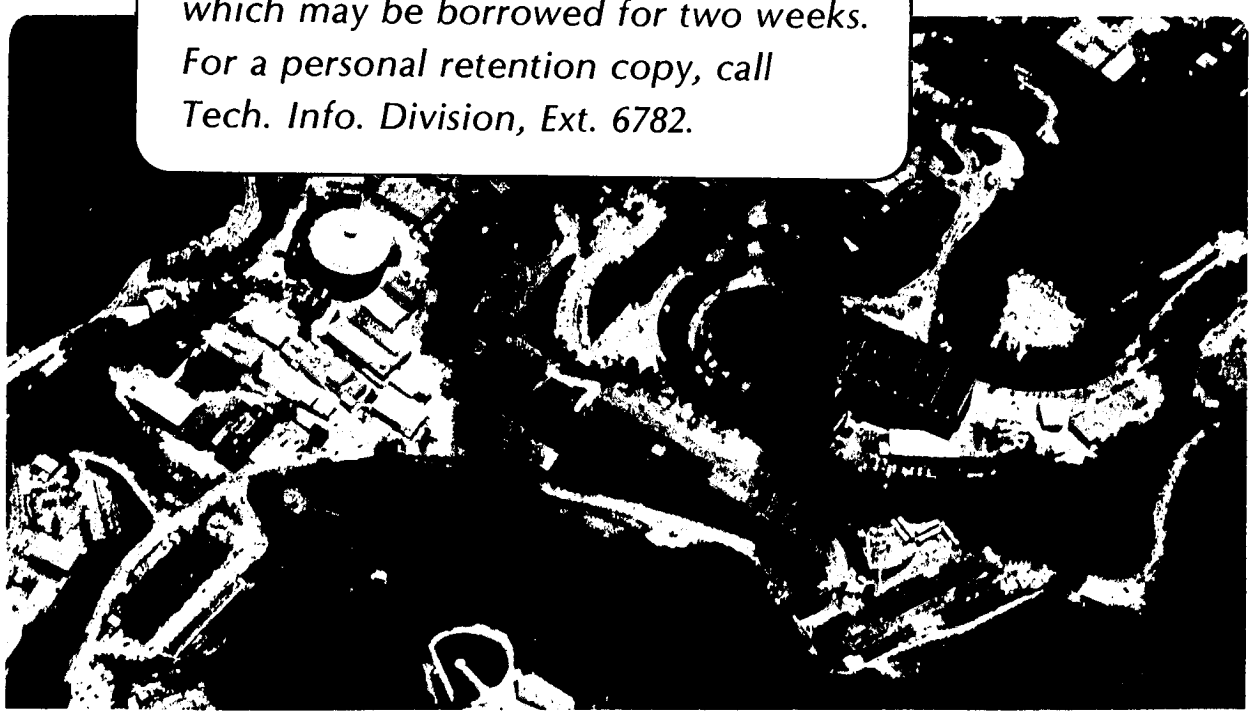

Prepared for the U.S. Department of Energy under Contract DE-AC03-76SF00098

DISCLAIMER

GATED TIME PROJECTION CHAMBER*

Peter Némethy and Piermaria J. Oddone

Lawrence Berkeley Laboratory
University of California
Berkeley, CA 94720

Nobukazu Toge and Akira Ishibashi

Department of Physics
University of Tokyo
Tokyo 113, JAPAN

ABSTRACT

We describe test results on the operation of a gated Time Projection Chamber. Symmetric pulses of ±120V, applied to alternate wires of a gating grid, turn the detector from an insensitive state to a sensitive state without impairing the readout of the chamber for more than 2.5 μs.

---

* This work was supported by the U.S. Department of Energy Contract DE-AC03-76SF00098 and by the Joint Japan U.S. Collaboration in High Energy Physics.

1. Introduction

A Time Projection Chamber, or TPC, is a drift chamber with no detector elements in the active volume [1]. A long drift region is followed by multiwire proportional chamber sectors where wire signals and associated cathode pad signals provide 3-D trajectories and dE/dx.

The build-up of positive ions in the drift volume places a serious limitation on the operation of continuously sensitive Time Projection Chambers in high-rate or high-background environments. The ions, generated in the proportional multiplication process at the sense wires, feed back into the drift volume. There they build up a space charge cloud which may significantly distort the projected tracks in the chamber. In the PEP-4 TPC we observed distortions of several millimeters from positive ions at PEP luminosities of 10^{31} cm^{-2} sec^{-1}.

Operating the TPC in a gated mode offers a fundamental solution to the positive ion problem [2,3]. A gating grid placed between the drift and proportional multiplication regions is normally kept opaque so that electrons do not reach the sense wires. No ions are generated or collected during this "gate closed" time. When an external pretrigger signals a potentially interesting event, the gating grid is pulsed to become transparent for the time that it takes for the electrons of the event to reach the sense wires. The positive ion flux reaching the drift volume can be reduced by several orders of magnitude in such a scheme. While the TPC cannot be used in the pretrigger decision, the data for triggered events are acquired as in a normal, continuously sensitive TPC, and the information obtained from the TPC is available to make subsequent readout decisions.

We have developed and tested a practical configuration for an event gated Time Projection Chamber.

2. Design

The operating principle of the gated TPC is shown in Fig. 1. On their way to the anode sense wires, the ionization electrons drift through a pair of grids. The first is a pulsed gating grid, the second a shielding grid protecting the sense wire and pad electronics. In analogy with vacuum tube nomenclature we call this device a "Tetrode TPC" in contrast with a standard "Triode TPC" (such as PEP-4) in which a single grid separates the drift region from the anode wires.

Alternate wires of the gating grid (GG) are connected to two separate voltage sources (Fig. 1). The transparency of the GG plane is controlled by changing the GG wire potentials.

$$V_{G1} = \bar{V}_G + \Delta V_G(t)$$
$$V_{G2} = \bar{V}_G - \Delta V_G(t)$$

where $\bar{V}_G$ denotes the average potential of all the GG wires (constant in time), and $2\Delta V_G$ gives the potential difference between the two groups of GG wires (varying with time). The value of ΔV_G is normally such as to prevent ionization electrons from reaching the sense wires. When an event is detected, ΔV_G is quickly switched to zero, making the gate fully transparent.

In this event-gated mode, the switching time (including the recovery of the electronics) must be kept short compared to the electron drift time (typically 20 μs for a 1 m long TPC). In this way only an early time slice is lost for the event, and the reduction of the fiducial length of the TPC is

minimized. The signal induced on the sense wires and cathode pads must therefore be kept small to avoid overloading the femto-coulomb sensitivity wire and pad electronics at the start of the event.

Two measures are taken to control the sense wire and cathode pad pickup. The gating grid is pulsed symmetrically (Eq. 1) in order to give first order cancellation of the signal induced by GG1 and GG2. The residual pickup, which would still be quite violent in a Triode TPC, is further attenuated by the thoroughly grounded shielding grid placed between the gating grid and the sense wires (Fig. 1). This second grid is essential to the success of such a gating scheme.

In applications with narrow beam pulses separated by large intervals a gated TPC can be operated synchronously [2,4]. The TPC is turned on for each beam pulse and is kept off between beam pulses. In this mode the TPC is switched well before an event of interest is detected, and recovers fully before the event. Thus, positive ions are suppressed without any loss of fiducial volume. The Tetrode TPC can also be operated in this synchronous, technically less demanding mode.

3. Test Apparatus

We performed our tests on a spare sector (Fig. 2) of the PEP-4 TPC. A sector is one of 12 proportional chamber assemblies (6/endcap) of the TPC.

The sector, originally a standard Triode TPC, was modified for this test, as shown in Fig. 3. The original grid (part of the sector) was solidly grounded to the preamplifier ground plane, to serve as a shielding grid. The gating grid was wound on an external, independent aluminum frame, made of

square box beams. The gating grid frame was attached to the sector on standoffs. The adjustable distance between shielding and gating grids was controlled to 200 μm. Above the gating grid a foreshortened drift region was defined by a mesh electrode, which we will call a "tower". Finally a field cage of rings, controlled by a resistor chain, ran around the periphery of the sector. Table 1 shows the parameters of the sector, gating grid, and tower.

A Fe^{55} line source, illuminating all wires, was placed above the tower to provide ionization electrons (from the conversion of 6 KeV X-rays) in the drift region. The whole assembly was placed in a high pressure vessel and operated in conditions identical to the PEP-4 TPC, listed in Table 2. The ionization signals and GG pulsing pickup were observed with standard PEP-4 TPC amplifiers, a combination of hybrid preamps [5] and discrete shaper amps. In addition, the sense wire and tower currents were measured with high-sensitivity ammeters.

4. Performance: Electron Drift Tests

To establish the operating conditions of the gated grid, we observe the sense wire and towers currents, i_S and i_T, with DC potentials V_{G1} and V_{G2} applied to the gating grid (Eq. 1). The tower is isolated from the field cage resistor chain. Therefore, the currents i_S and i_T, induced by the Fe^{55} source, directly measure the electon and positive ion currents, respectively.

With $\Delta V_G = 0$ we obtain the potential $\bar{V}_G$ (Eq. 1) needed for the open gate. Figure 4(a) shows i_S vs $\bar{V}_G$ for a distance $d = 4.3$ mm

between gating and shielding grids. The plateau, corresponding to 100% electron transmission, is reached at $\bar{V}_G \simeq -600$ V. At this voltage the ratio of bulk electric field in front (E_F = 600 V/4.3 cm) to the drift electric field in back (E_B = 7.5 KV/m) is $E_F/E_B = 1.9$. For d = 6.3 mm the plateau shifts to the right by about 150 V; $E_F/E_B = 1.9$ again. These results are in good agreement with the conformal mapping calculations of Bunemann [6] which predict $E_F/E_B \sim 2$ for full transparency with our grid parameters. This transparency condition is also satisfied at the shielding grid because of the high voltage ($V_S \sim 4$ kV) on the sense wires.

The fraction of positive ions reaching the drift volume with the gate open, measured by the ratio i_T/i_S, is 20% for d = 4.3 mm and 13% for d = 6.3 mm.

To close the gate we increase ΔV_G while holding $\bar{V}_G = -700$ V (for d = 4.3 mm). Figure 4(b) shows i_S vs ΔV_G. The grid is completely opaque for $\Delta V_G \gtrsim 100$ V. Table 3 summarizes the potentials on G1 and G2 for open and closed conditions.

For fast pulsing of the gating grid at these potentials, we developed a simple switching circuit, shown in Fig. 5. The photocouplers control high-power VMOS FET's. When the FET's are turned off, GG_1 and GG_2 remain at the values of HV_1 and HV_2. When the FET's are turned on, GG_1 and GG_2 are pulled down to HV_3. Figure 6 shows typical switching pulse shapes on GG_1 and GG_2 from this circuit. An oscilloscope trace of the front end of a gating pulse, and of the assymetry between the gating pulses, is shown in Fig. 7. The voltage mismatch at turn-on is typically less than 2% of the total switching amplitude.

Pulse height spectra from the line source (on an arbitary sense wire), taken while pulsing the grid, are shown in Fig. 8. The Fe^{55} spectrum looks normal during the event gate (Fig. 8 (a)) and is absent outside it (Fig. 8 (b)). The two spectra are normalized to the same live time; the gate off background (less than 1%) is due to ionization deposited beneath the gating grid.

The double pulse experiment of Fig. 9(a) measures the transit time of positive ions between sense wires and gating grid. The positive ion current i_T is observed while varying the separation t between pulse 1 and pulse 2 (with period T and pulse width τ fixed). Figure 9(b) shows the data. One peak corresponds to ions generated during gating pulse 1 passing through the grid on gating pulse 2 (transit time = t), the other peak to ions from pulse 2 passing through on the next pulse 1 (transit time = T - t). The two fold ambiguity is removed by repeating the experiment with a different period T. The transit time spread is obtained by twice unfolding the gate width τ from the observed width of the peak in i_T. Table 4 gives the results of this experiment, for two distances between the shielding and gating grids.

Since their transit time is long compared to the 20 μs event gate length, positive ions generated during one event can only enter the drift region when they arrive in accidental coincidence with a second event. For a finite duty factor D positive ions from random backgrounds are therefore suppressed by D^2, ions from the triggering events by D. Thus, a 500 Hz trigger rate (1% duty factor) gives a suppression of 10^{-4} and 10^{-2} for random and event generated ions, respectively.

5. Performance: Pulse Pickup

The signal induced on a sense wire, from switching the gate at the start of the event, can be decomposed into external, inductive, or capacitive pickup,

$$S = A_1 V + A_2 M \frac{di}{dt} + A_3 \delta(CV), \qquad (2)$$

where S is the preamplifier signal in mV, V is the gate switching voltage and i is the gate switching current.

The importance of a given pickup amplitude is determined by the parameters of a TPC. With its choice of low wire gain (Table 2) and correspondingly high electronic gain the PEP-4 TPC is especially sensitive to pickup. In PEP-4, minimum ionizing tracks make a 15 mV signal from the 50 femto-coulomb charge deposited on a wire. The preamp dynamic range is 2000 mV.

An example of external pickup (term A_1 in Eq. 2) is the direct coupling of either busbar to the sense wire artwork or preamps. We observe it at a signal level $S \sim 10$ mV. We see no evidence for other sources of external pickup, such as the motion of the ground away from zero volts. We note that, even though we switch large currents (typically 1 ampere) the switched charge moves from one half of the gating grid to the other (Fig. 10 (a,b)), and no net current flows into the ground.

When the gating grid is pulsed with busbars on either side (Fig. 10 (c)), inductive pickup (term A_2 in Eq. 2) dominates, with S as big as 600 mV. We identify this term by its characteristic signature. Since $M \propto \ell$ and $q \propto C \propto \ell$, $M\, di/dt \propto \ell^2\, d^2V/dt^2$, where ℓ is the wire length. This is the behavior we observe. The dominance of the inductive pickup in this configuration can be understood with the aid of Fig. 10(c). The plus/minus pulsing of the gating grid provides voltage, but not current

cancellation, since all charging currents flow in the same direction on the grid wires. The problem is remedied by running both grid halves from busbars on the same side (Fig. 10 (d)) so that counter-flowing currents cancel to first order. Indeed, we see no evidence of inductive pickup in this geometry, which is our choice. In this case the capacitive pickup (term A_3 in Eq. 2) dominates.

The sensitivity to capacitive pickup is measured by a deliberate 10% mismatch of the gating pulses. Figure 11 shows the resulting preamp pickup signal versus wire number. The graph shows the correct signature, $S \propto \ell$, for capacitive pickup, and can be parametrized as

$$S = 40\ \text{mV} \times \ell\,(\text{m}) \times \text{mismatch}\ (\%)\ . \qquad (3)$$

This sensitivity corresponds to an improvement, over the measured pickup in a pulsed triode TPC, of a factor of 26. This factor is composed of a factor of 2 due to the increased distance between gating grid and sense wires and a factor of 13 due to the shielding grid.

The capacitive pickup can be expanded into

$$\delta(CV) = V\delta C + C\delta V\ . \qquad (4)$$

The difference capacitance term comes from imperfect geometry; the difference voltage term from imperfect matching of the plus/minus pulse shapes. Figure 12 is a scope trace of the preamp output on one of the long wires, for our best tune of the pulser. The early fast pulses come from the voltage mismatch, the long tail is from the capacitance difference.

Figure 13 shows the pickup size vs wire number, from each of these terms, again for our best pulser tune. Except for places of known geometrical asymmetry (first and last wires, where the grids end, and the "kite corner", where the wire length changes are irregular) the pickup from both sources is less than 80 mV, implying with Eq. 3, that

$$\delta V/V \sim 2\% \quad (5)$$

$$\delta C/C \sim 2\% \quad (6)$$

Equation (5) is in good agreement with the observed pulser asymmetry (Fig. 7). A pulser with better tracking of the plus/minus signals would be worthwhile.

The 2% difference capacitance of Eq. (6) is insensitive to the global placement of the TPC elements. Down to a level of 0.2%, we observe no changes in $\Delta C/C$ from changing the spatial phase between sense wires, shielding grid wires and gating grid wires. Nor do we see an effect from variations in the height, parallelism and overall twist of the gating grid by up to 200 μm or from rotations crossing the gating and shielding grids by up to 2 wires. The difference capacitances appear to be dominated by local tolerances, not global ones.

The scale of the capacitive pickup signal on the sense wires (~60 mV) is about four times the minimum ionizing signal but only 1/35 of the preamp dynamic range. Therefore, the pickup does not pose any danger of preamp saturation and "lockout" during a long recovery time. Pickup on the cathode pads is smaller by an order of magnitude.

Figure 14 shows the pickup signal at the shaper amp output; it uses up all of the shaper amplifier dynamic range (2V) during the first 2 μs; ionization signals from tracks can be observed only after that time. Inclusion of a trigger decision time of 500 ns gives a loss of 2.5 μs at the start of the event. For the PEP-4 drift velocity (Table 2) this translates to a reduction of 12.5 cm in the TPC fiducial length at each endcap.

6. Conclusions

The pulsed tetrode scheme of gating a Time Projection Chamber is a viable method of avoiding track distortions from positive ions in the TPC.

In an event gated mode an external trigger is required and the 2.5 μs recovery time leads to some reduction of the TPC fiducial volume. Gated operation will yield very large reductions in positive ion feedback, even for relatively big duty factors. At a low repetition rate accelerator, a beam-gated mode will lead to the complete suppression of ion feedback with no accompanying loss of the TPC volume.

Gated operation thus extends the application of Time Projection Chambers to high rate and high background experiments.

We thank Shawn Carlson for contributions to the early phases of this work, Ray Fuzesy for winding the gating grid plane, Don Blackman and Doug Shigley for machining work, and Gerry Przybylski for discussions on electronics circuitry.

This work was supported by the U.S. Department of Energy Contract DE-AC03-76SF00098 and by the Joint Japan U.S. Collaboration in High Energy Physics.

References

1. D. Fancher, et al., Nucl. Instr. and Meth. 161, 383 (1979); see also Proposal for a PEP Facility Based on the Time Projection Chamber, Johns Hopkins University, Lawrence Berkeley Laboratory, UCLA, UC-Riverside, and Yale University (PEP Exp. 4), LBL Pub. 5012 (1976).
2. D.R. Nygren, Physica Scripta 23, 584 (1981); D. Friedrich et al., Nucl. Instr. and Meth. 158, 81 (1978).
3. For a discussion of the gating of multistep avalanche chambers, and of high pressure drift detectors, see A. Breskin et al., Nucl. Instr. and Meth. 178, 11 (1980); I. Lehraus et al., Nucl. Instr. and Meth. 197, 361 (1982).
4. An example is the SLAC Linear Collider (SLC) with a 180/sec repetition rate and a few ps pulse length. See SLAC Linear Collider Conceptual Design Report, SLAC Report-229 (1980); Letter of Intent: The PEP-4 Facility (TPC) as the Initial Detector at SLC, Ames Laboratory, Iowa State University, Johns Hopkins University, Lawrence Berkeley Laboratory, UCLA, UC-Riverside, and University of Massachusettts (1982, unpublished).
5. D. Landis et al., IEEE Transactions on Nucl. Sci., NS29, 573 (1982).
6. O. Bunemann et al., Canadian Journal of Research A27, 191 (1949).

Figure Captions

Fig. 1. Electric field configurations in gated TPC.

Fig. 2. Photograph of PEP-4 TPC Sector.

Fig. 3. Cutaway view of gated TPC test setup.

Fig. 4 (a) Sense wire current vs mean gating grid potential;

(b) Sense wire current vs grid closing potential.

Fig. 5. Schematic diagram of gating grid pulser.

Fig. 6. Pulser output signals.

Fig. 7. Oscilloscope trace of one gating grid pulse (vertical scale = 50 V/division) and of the difference between the two pulses (vertical scale = 2V/division). Horizontal scale is 1 μs/division.

Fig. 8. Pulse height spectra from Fe^{55} source inside and outside the event gate.

Fig. 9. (a) Timing diagram for double pulse experiment;

(b) Positive ion current vs gate separation.

Fig. 10. Charge distribution and charge flow on gated grid.

Fig. 11. Preamp pickup signal vs wire number for 10% gating pulse asymmetry.

Fig. 12. Oscilloscope trace of preamp pickup signal on wire 144 for best asymmetry. Vertical scale = 50 mV/division, horizontal scale = 1 μs/division.

Fig. 13. Preamp pickup signal vs wire number for best asymmetry. Open symbols show contribution of the voltage mismatch, solid circles are from difference capacitances.

Fig. 14. Oscilloscope trace of shaper amplifier pickup signal on wire 144, for best asymmetry. Vertical scale = 500 mV/division, horizontal scale = 1 μs/division.

Table 1.

Physical Parameters of Gated TPC

Sense wire length	23 cm to 96 cm
Cathode - sense wire plane distance	4 mm
Sense wire plane - shielding grid distance	4 mm
Shielding grid - gating grid distance	4.3-6.3 mm
Shielding and gating grid wire spacing	1 mm
Shielding and gating grid wire diameter	75 μm
Sense wire-field wire spacing	2 mm
Sense wire/field wire diameter	20 μm/75 μm
Drift region length (for test)	25 mm

Table 2.

PEP-4 TPC Operating Conditions

Gas Composition	80% Ar, 20% CH_4
Gas Pressure	8.5 Atm.
Field Wire Voltage	700 V
Sense Wire Voltage (typical)	3.5 kV
Sense Wire Gain	1000
Minimum Ionizing Signal	3×10^5 electrons
Drift Field	75 KV/m
Drift Velocity	5 cm/μs
Drift Distance	1.0 m

Table 3.

Potentials for Gating Grid Operation

POTENTIAL	OPEN	CLOSED
$V(G_1)$	-700V	-580V
$V(G_2)$	-700V	-820V

Table 4.

Positive Ion Drift Times

GRID POSITION	t	$\sigma(t)$
distance (GG-SG) = 4.3mm	2.5ms	0.6ms
distance (GG-SG) = 6.3mm	4.3ms	0.7ms

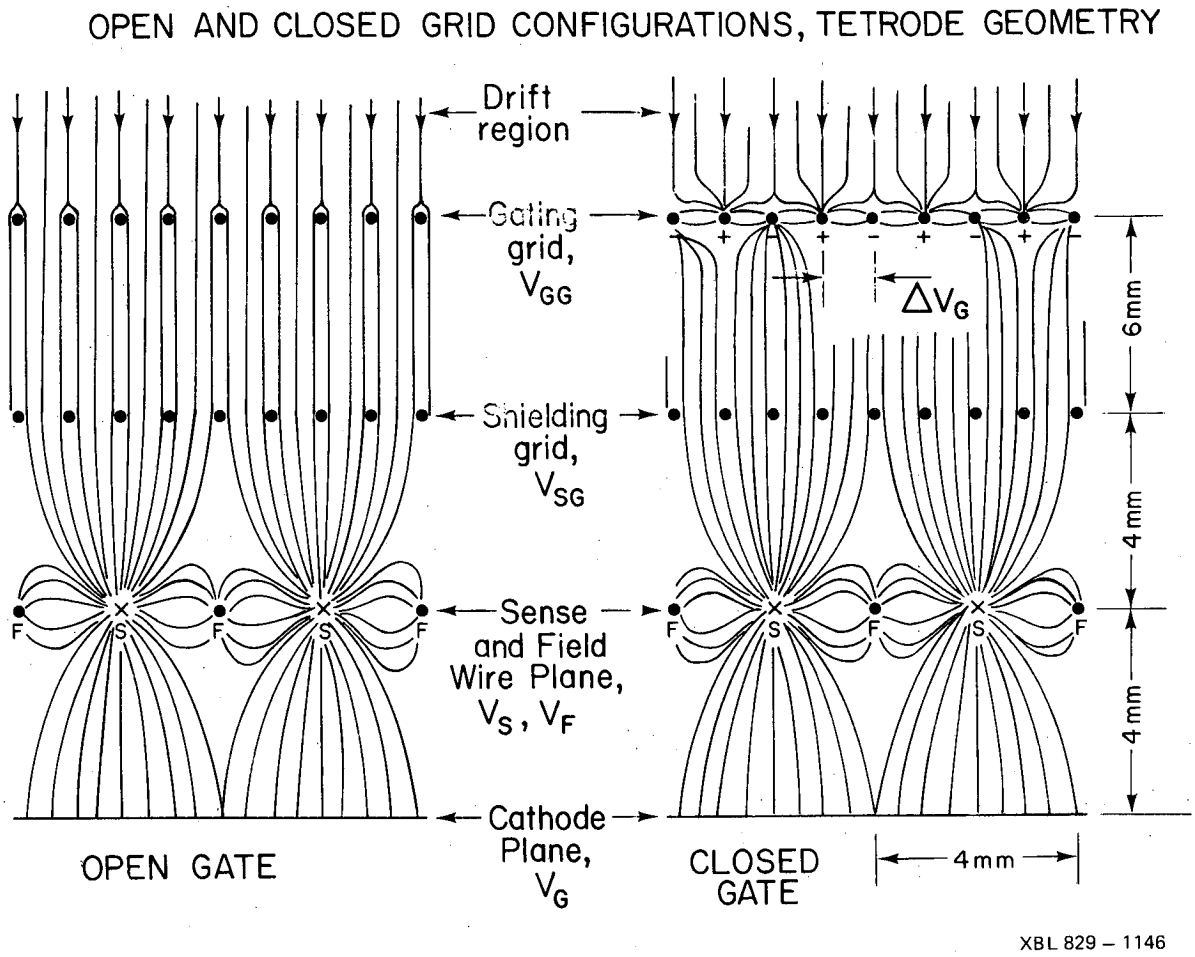
OPEN AND CLOSED GRID CONFIGURATIONS, TETRODE GEOMETRY
Drift region
Gating grid, V_{GG}
Shielding grid, V_{SG}
Sense and Field Wire Plane, V_S, V_F
Cathode Plane, V_G
ΔV_G
6mm
4 mm
4 mm
4mm
F
S
OPEN GATE
CLOSED GATE
XBL 829 – 1146

Fig. 1

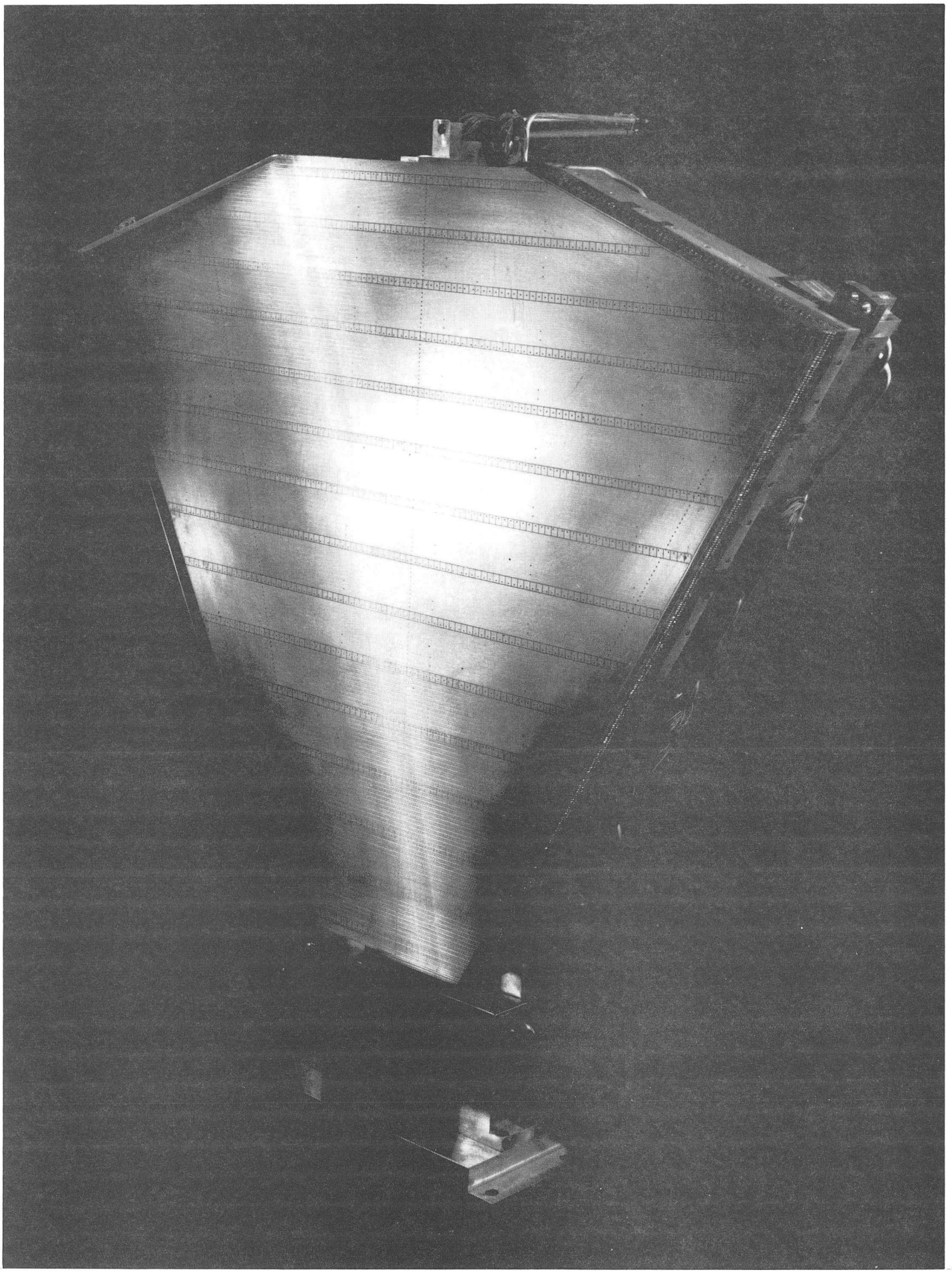

Fig. 2

CBB 817-6456

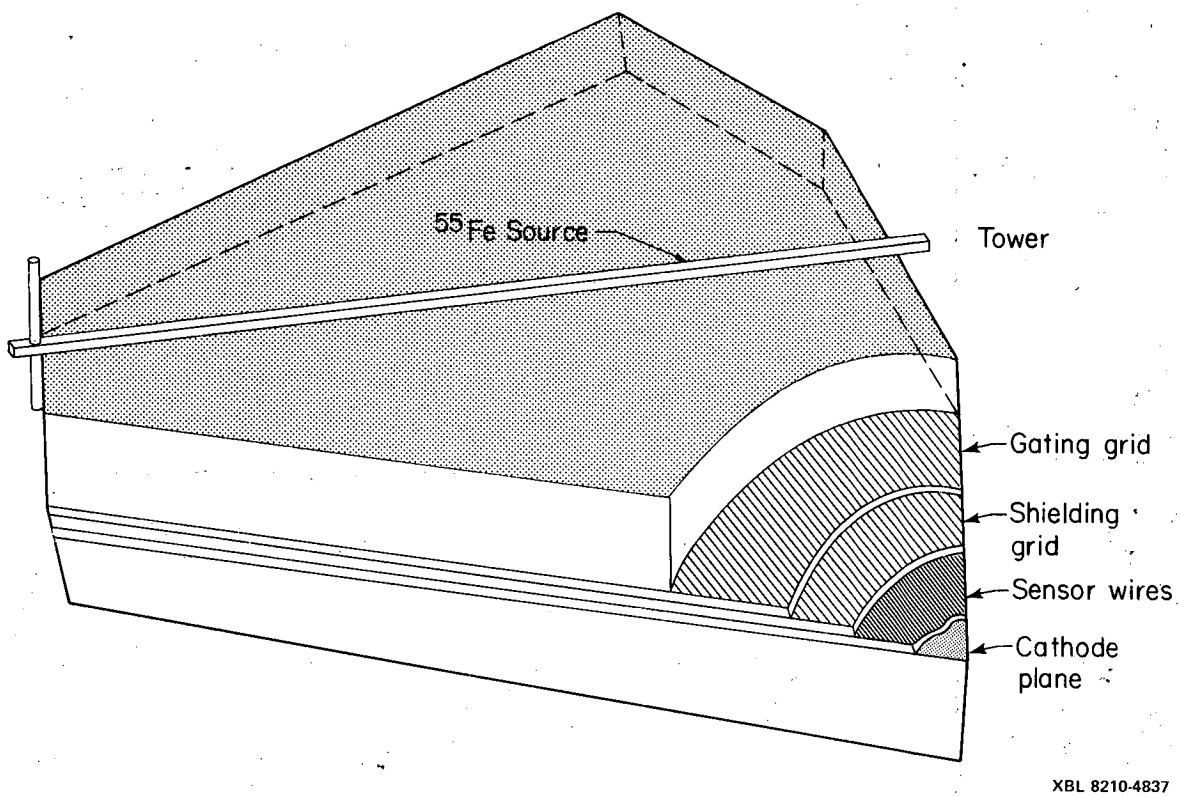
55Fe Source
Tower
Gating grid
Shielding grid
Sensor wires
Cathode plane
XBL 8210-4837

Fig. 3

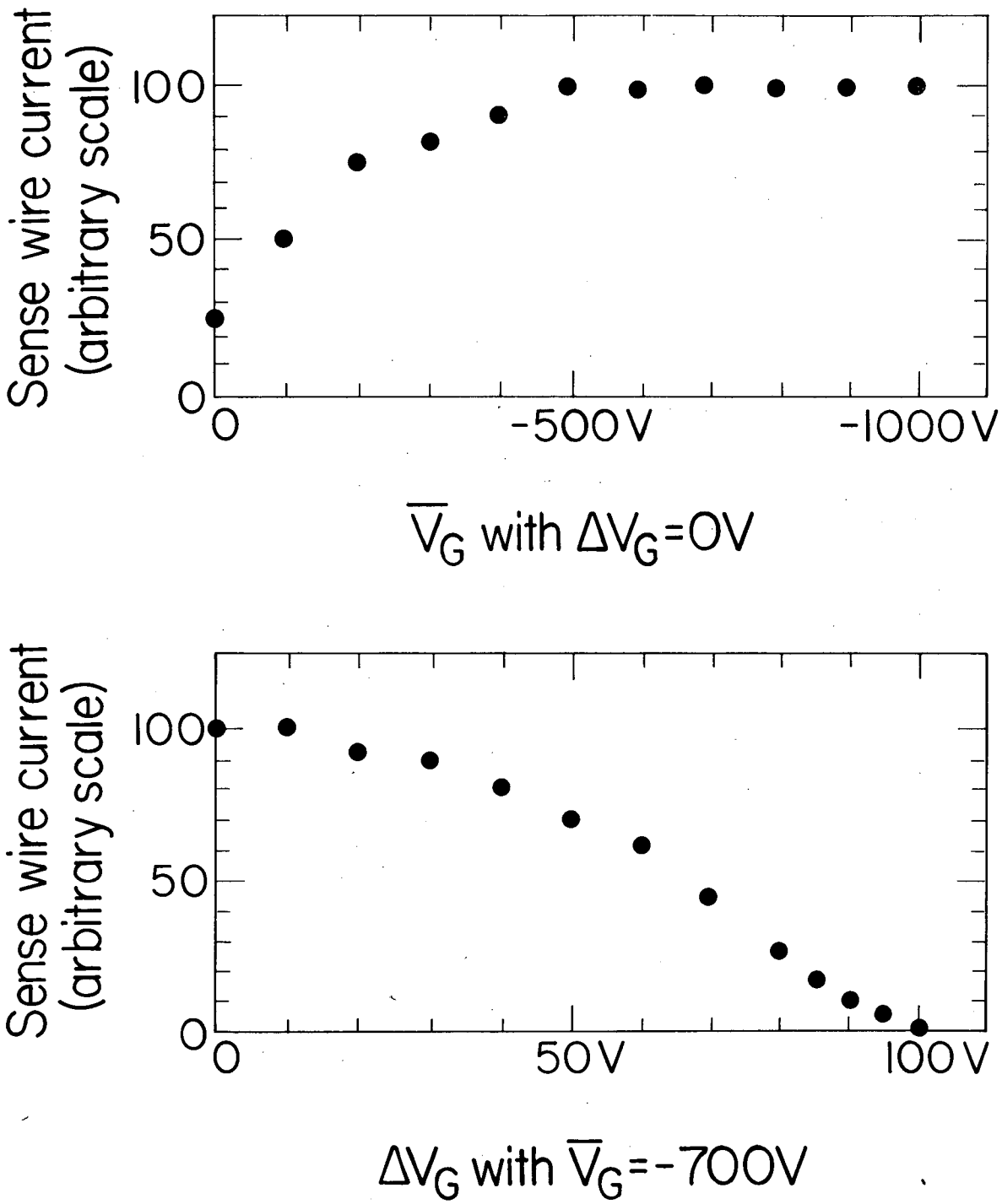
Sense wire current
(arbitrary scale)
100
50
0
0
-500V
-1000V
$\overline{V}_G$ with ΔV_G=0V
Sense wire current
(arbitrary scale)
100
50
0
0
50V
100V
ΔV_G with $\overline{V}_G$=-700V
XBL 8210-4833

Fig. 4

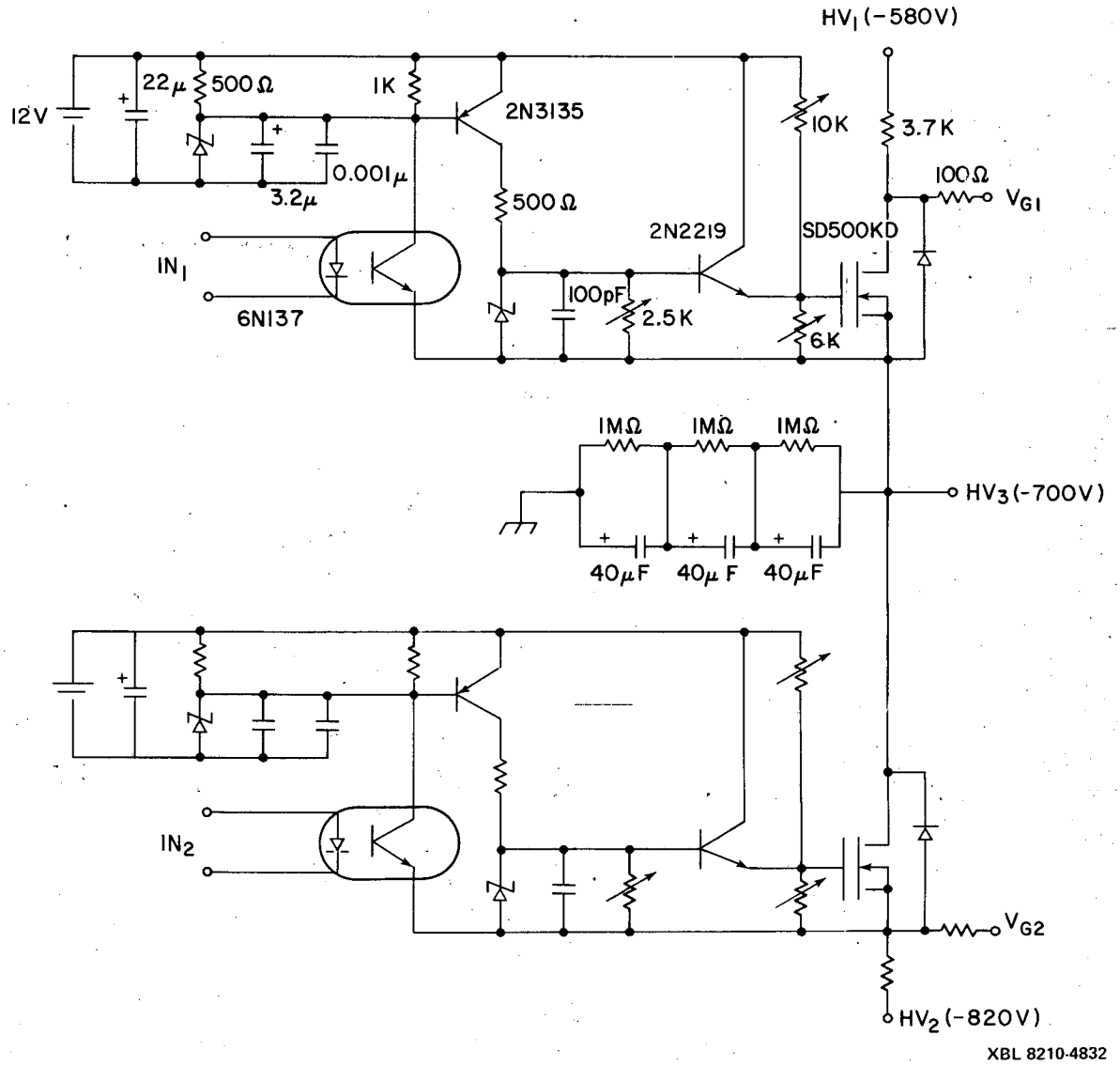
HV1 (-580V)
12V
22μ
500Ω
1K
2N3135
10K
3.7K
100Ω
VG1
0.001μ
3.2μ
500Ω
2N2219
SD500KD
IN1
6N137
100pF
2.5K
6K
1MΩ
1MΩ
1MΩ
HV3 (-700V)
40μF
40μF
40μF
IN2
VG2
HV2 (-820V)
XBL 8210-4832

Fig. 5

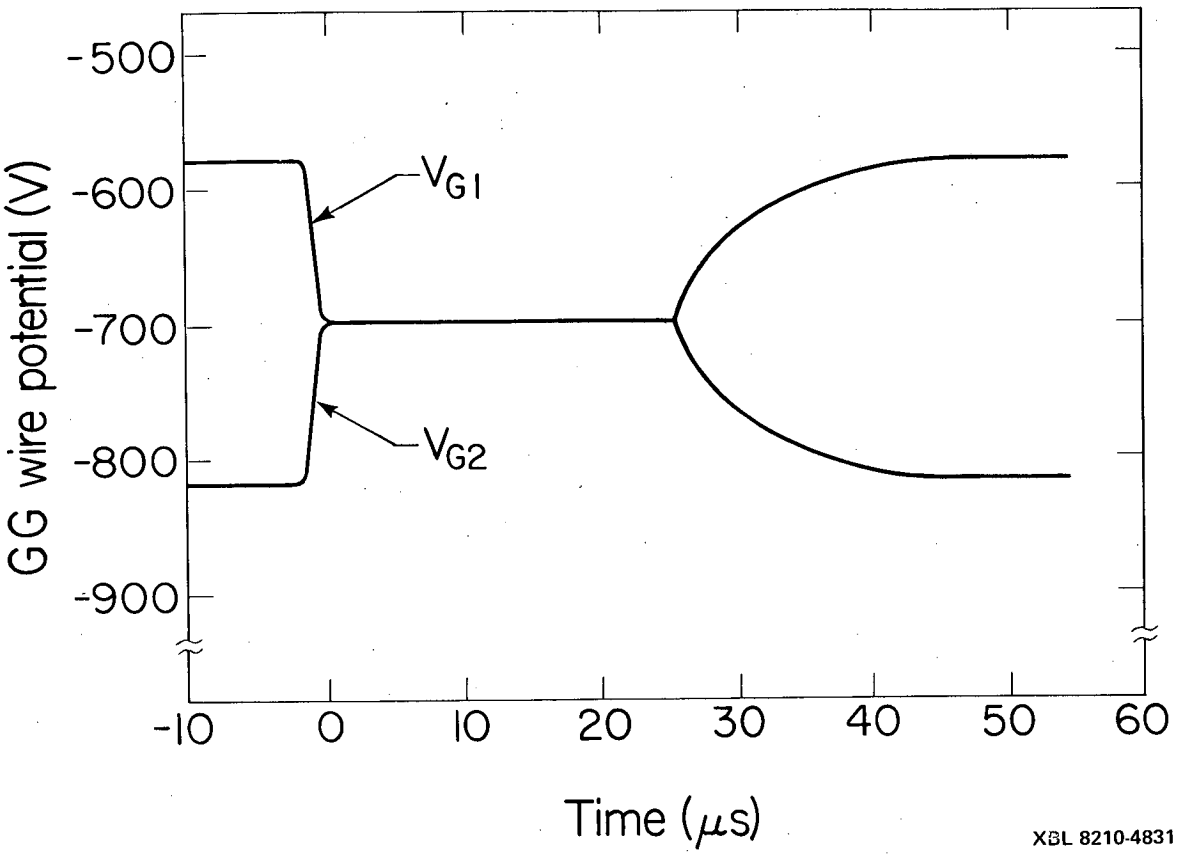
-500
-600
-700
-800
-900
GG wire potential (V)
V_{G1}
V_{G2}
-10
0
10
20
30
40
50
60
Time (μs)
XBL 8210-4831

Fig. 6

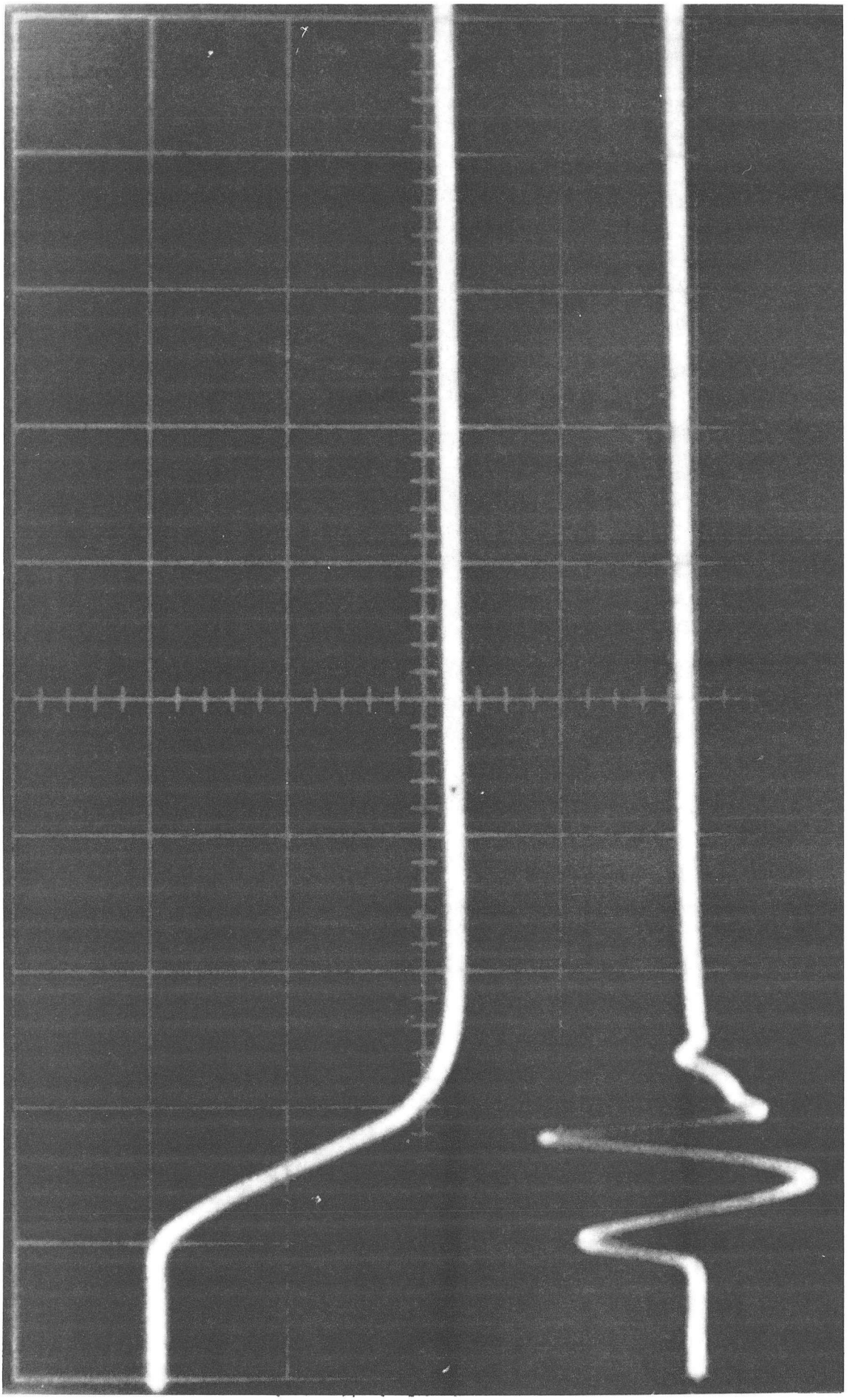

XBB 820-8860

Fig. 7

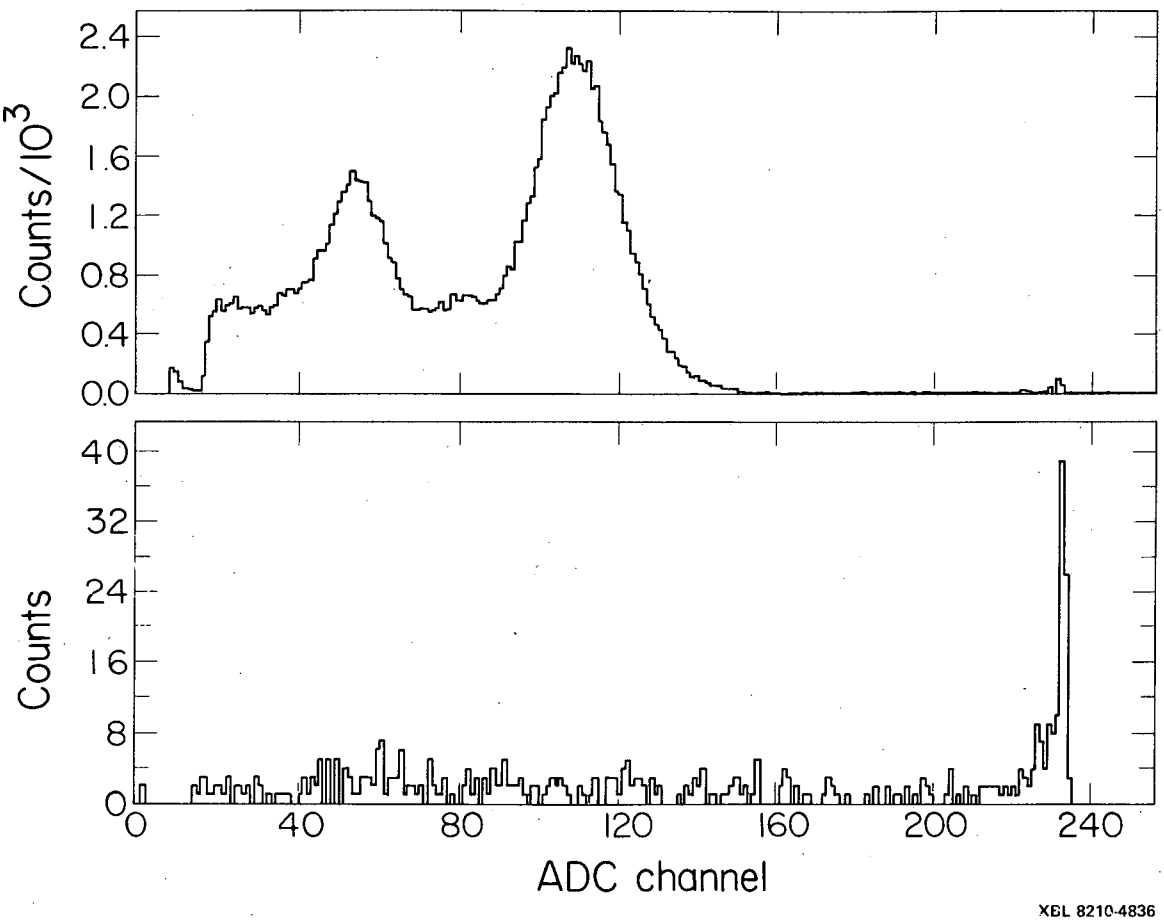
Counts/10^3
2.4
2.0
1.6
1.2
0.8
0.4
0.0
Counts
40
32
24
16
8
0
0
40
80
120
160
200
240
ADC channel
XBL 8210-4836

Fig. 8

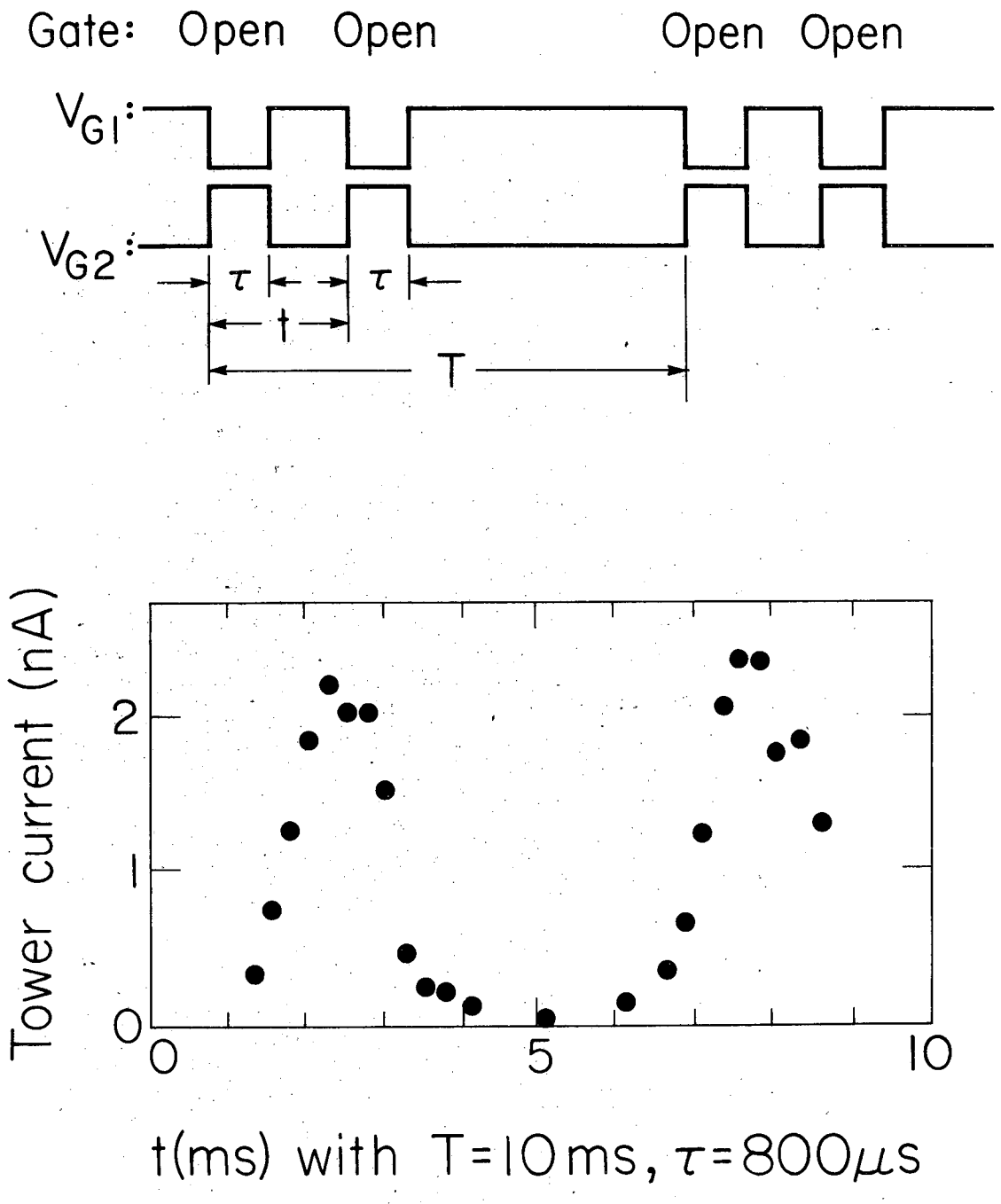
Gate: Open Open Open Open
V_{G1}:
V_{G2}:
τ
τ
t
T
Tower current (nA)
0
1
2
0
5
10
t(ms) with T=10ms, τ=800μs
XBL 8210-4849

Fig. 9

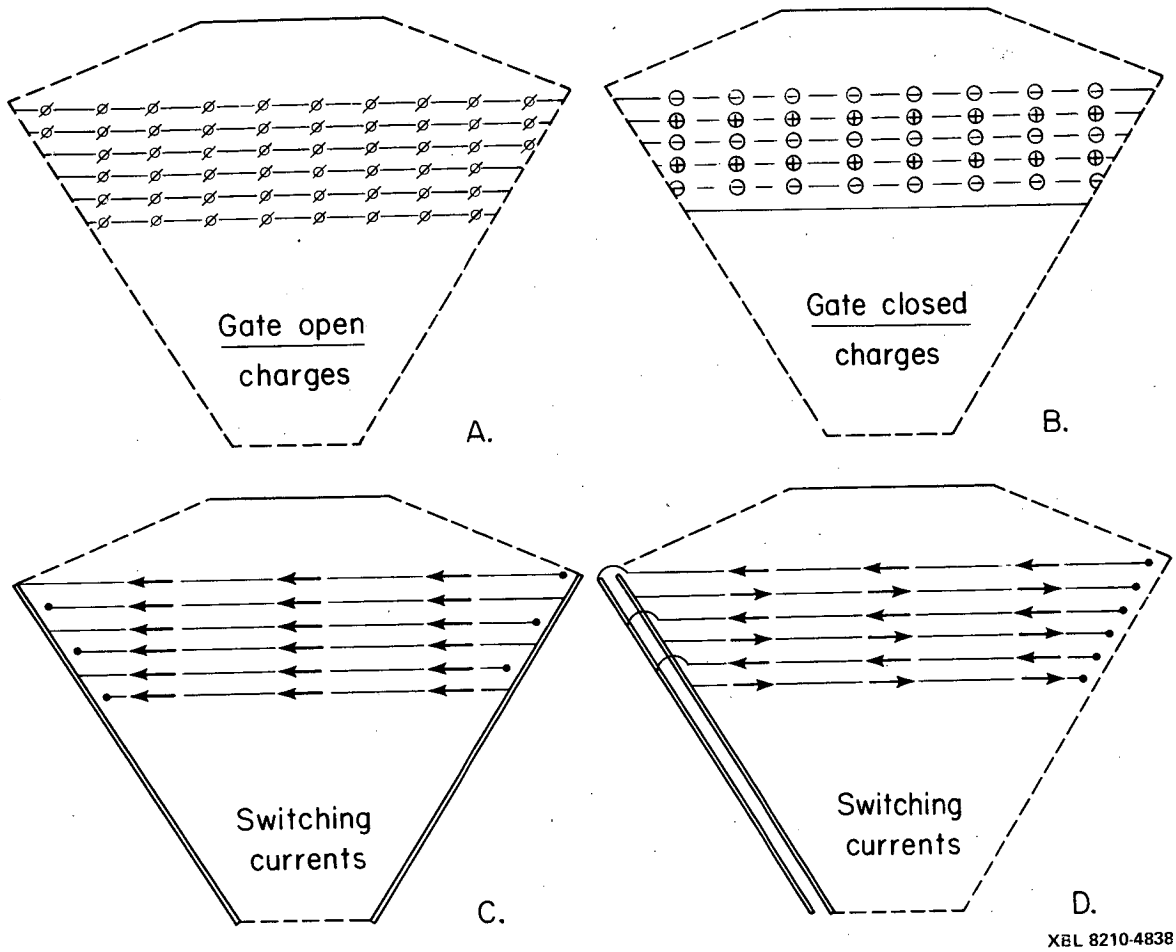
Gate open
charges
A.
Gate closed
charges
B.
Switching
currents
C.
Switching
currents
D.
XBL 8210-4838

Fig. 10

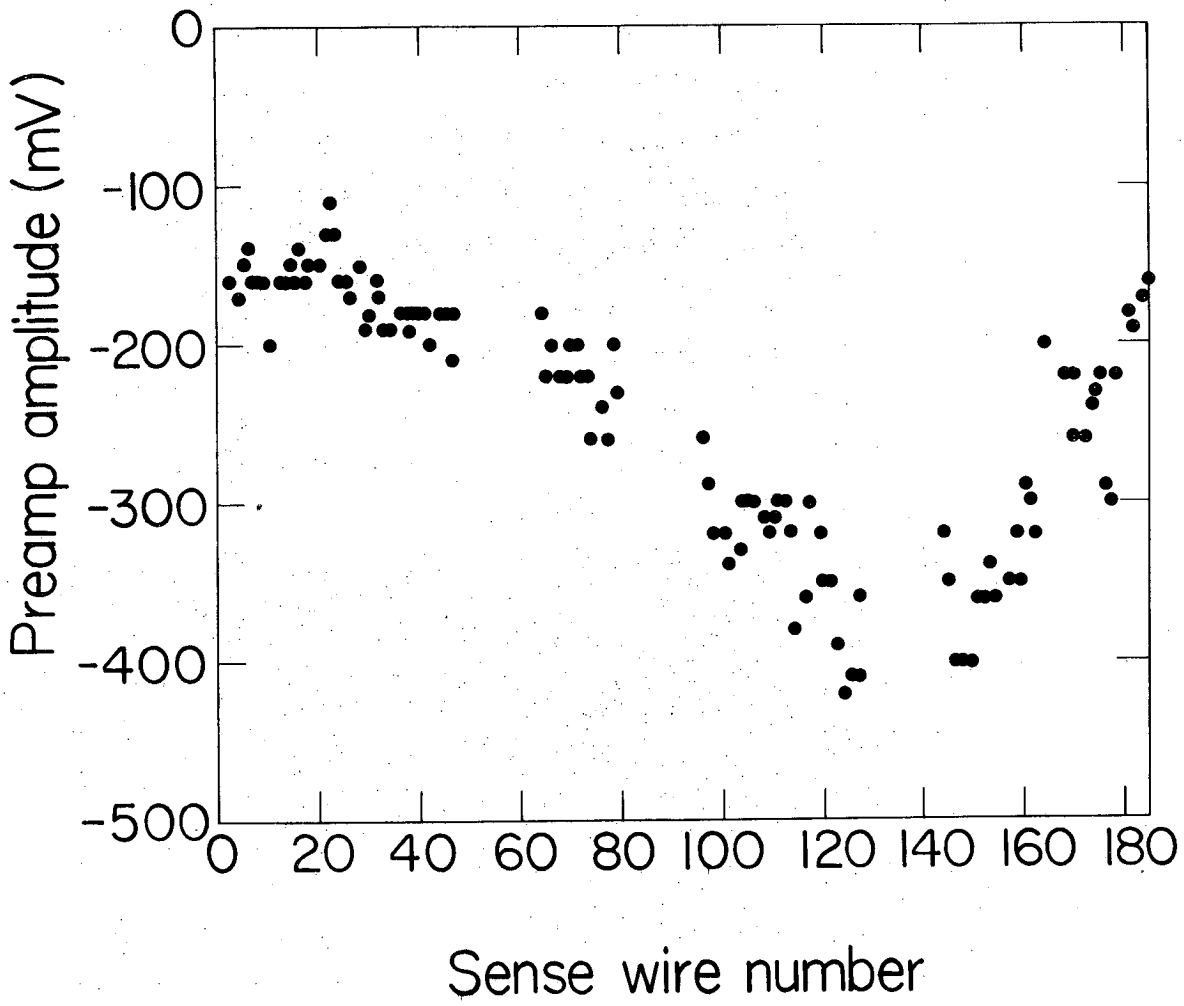
Preamp amplitude (mV)
0
-100
-200
-300
-400
-500
0
20
40
60
80
100
120
140
160
180
Sense wire number
XBL 8210-4834

Fig. 11

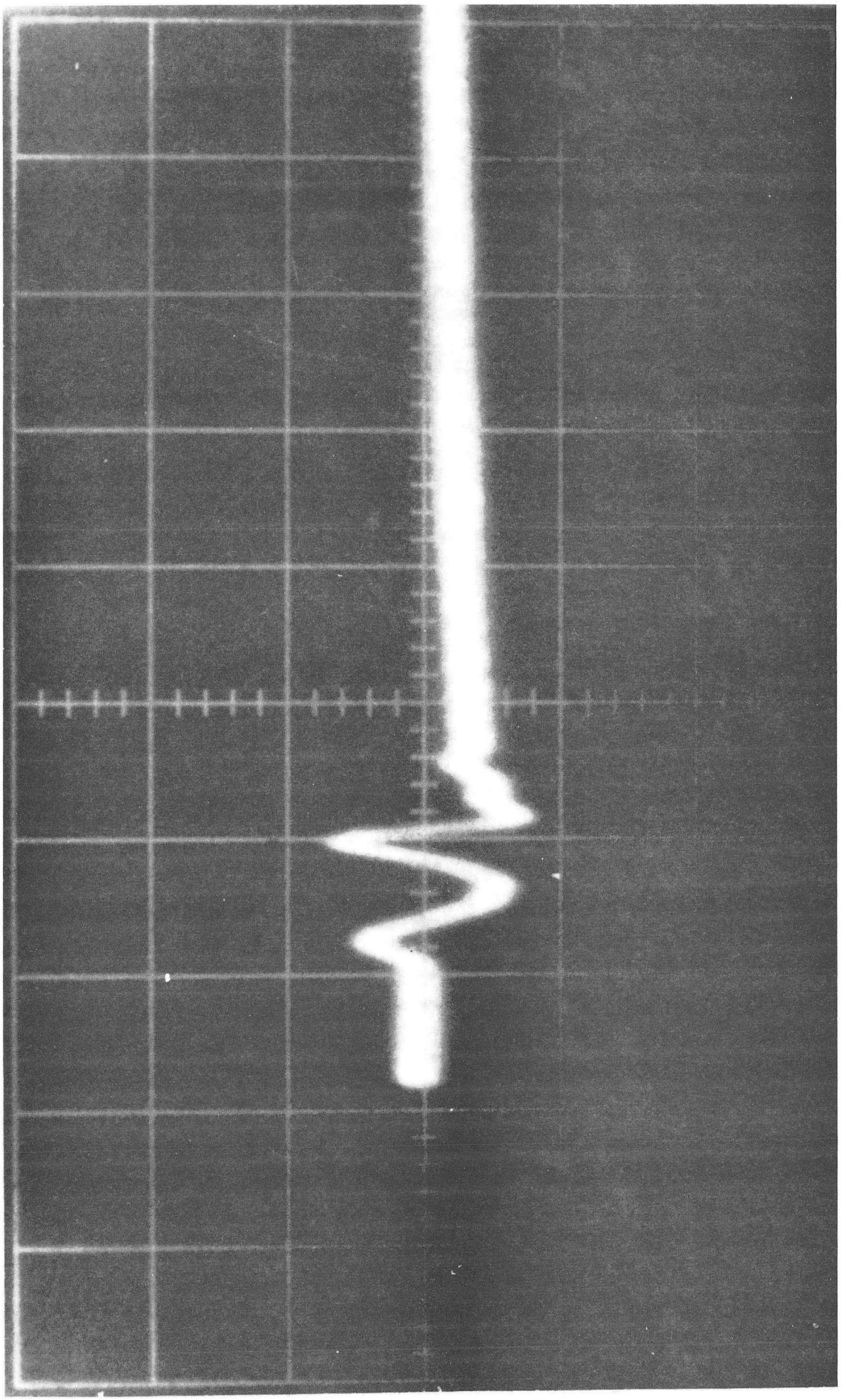

XBB 820-8859

Fig. 12

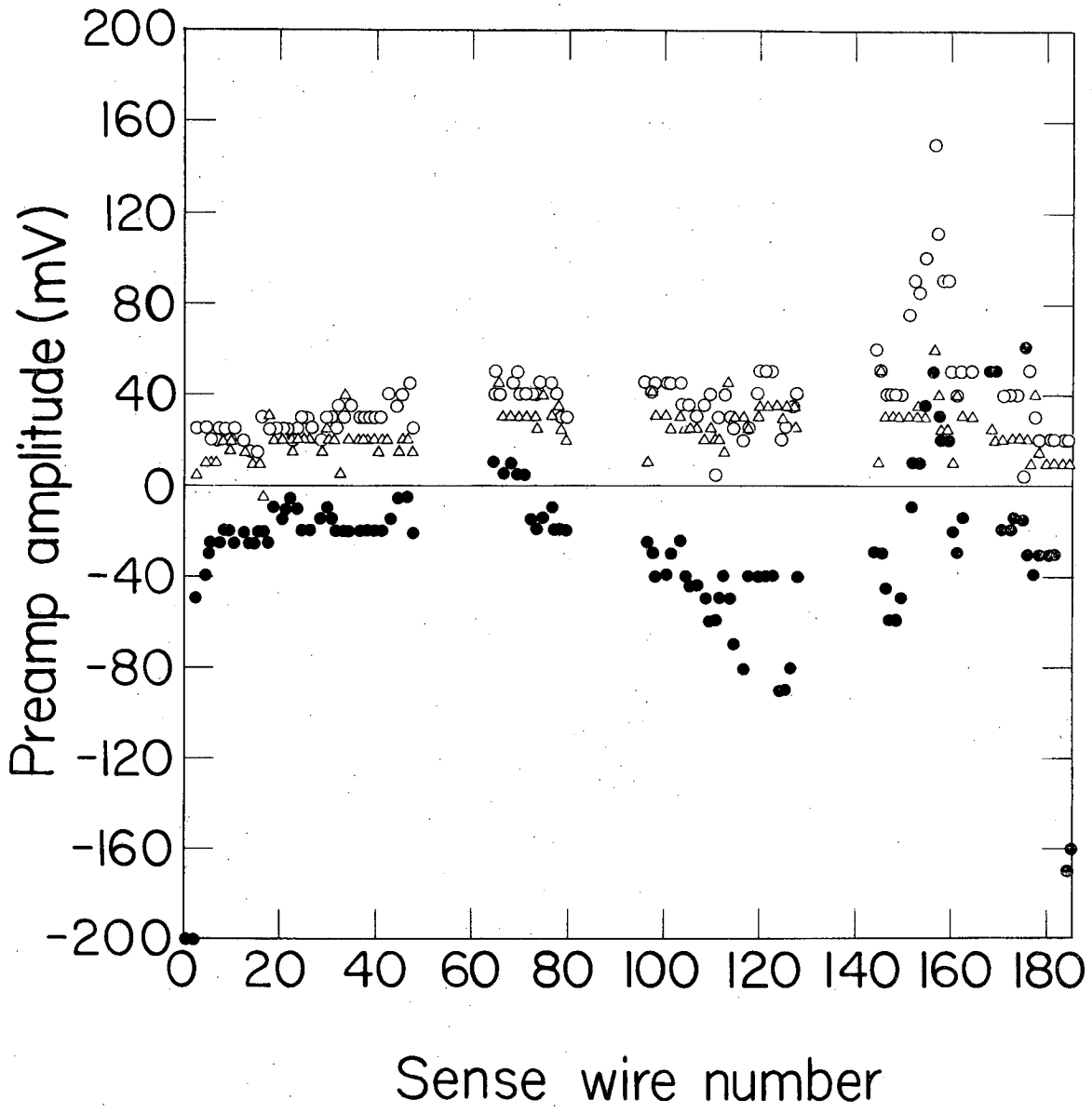
200
160
120
80
40
0
-40
-80
-120
-160
-200
Preamp amplitude (mV)
0 20 40 60 80 100 120 140 160 180
Sense wire number
XBL 8210-4835

Fig. 13

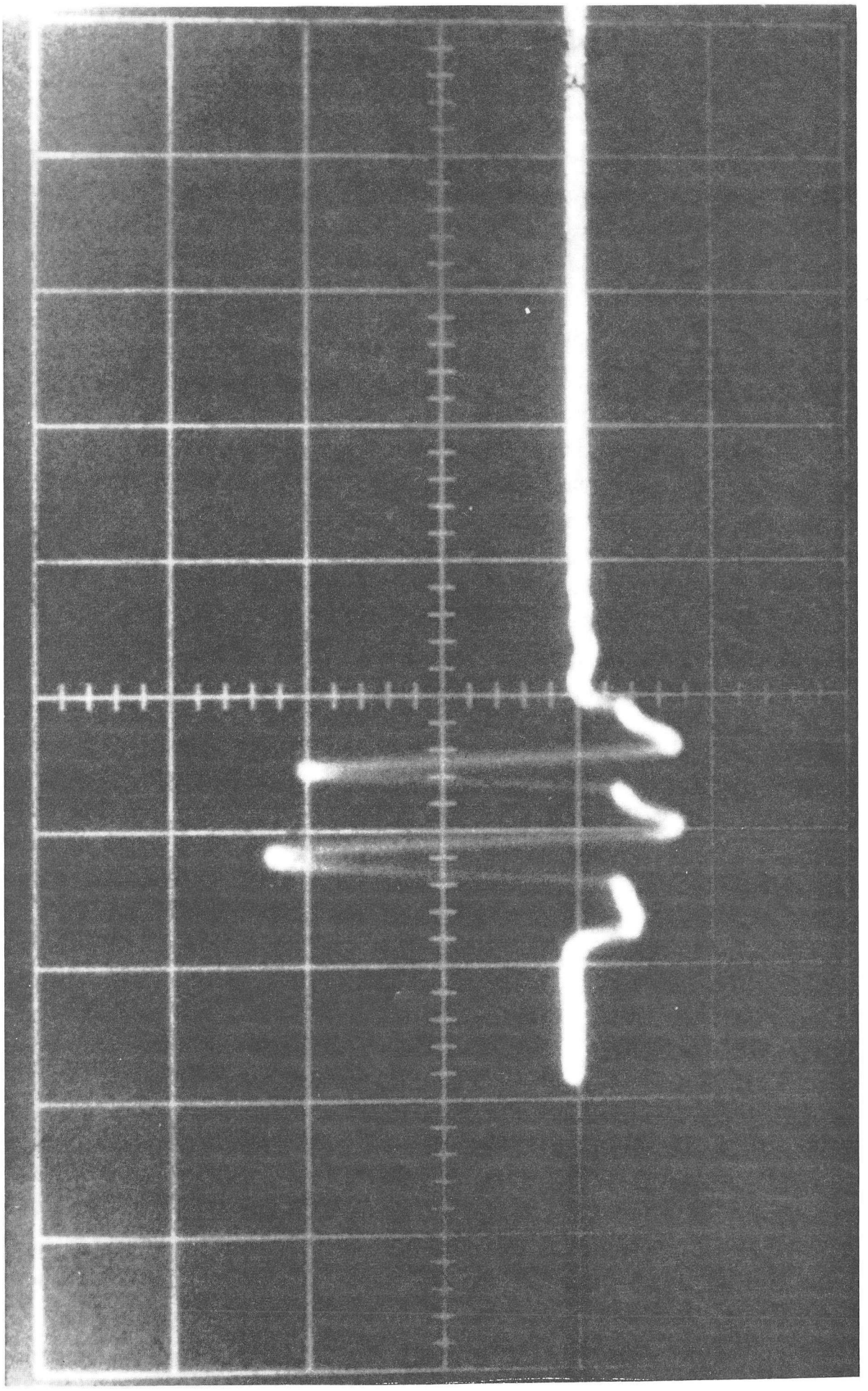

XBB 820-8861

Fig. 14

This report was done with support from the Department of Energy. Any conclusions or opinions expressed in this report represent solely those of the author(s) and not necessarily those of The Regents of the University of California, the Lawrence Berkeley Laboratory or the Department of Energy.

Reference to a company or product name does not imply approval or recommendation of the product by the University of California or the U.S. Department of Energy to the exclusion of others that may be suitable.

TECHNICAL INFORMATION DEPARTMENT
LAWRENCE BERKELEY LABORATORY
UNIVERSITY OF CALIFORNIA
BERKELEY, CALIFORNIA 94720